Journal of Power Sources 212 (2012) 148–153

Contents lists available at SciVerse ScienceDirect

Journal of Power Sources

journal homepage: www.elsevier.com/locate/jpowsour

Electrochemical Raman study of edge plane graphite negative-electrodes in electrolytes containing trialkyl phosphoric ester

Hiroe Nakagawa [a], Manabu Ochida [a], Yasuhiro Domi [a], Takayuki Doi [a,*], Shigetaka Tsubouchi [a], Toshiro Yamanaka [a], Takeshi Abe [b], Zempachi Ogumi [a]

[a] Office of Society-Academia Collaboration for Innovation, Kyoto University, Gokasho, Uji, Kyoto 611-0011, Japan
[b] Graduate School of Engineering, Kyoto University, Nishikyo-ku, Kyoto 615-8510, Japan

ARTICLE INFO

Article history:
Received 14 February 2012
Received in revised form
2 April 2012
Accepted 5 April 2012
Available online 13 April 2012

Keywords:
Flame retardant
Graphite
Edge plane
Intercalation
Raman spectroscopy
Lithium-ion battery

ABSTRACT

Structural changes in the surface of edge plane graphite electrodes were studied in ethylene carbonate-based electrolytes containing a flame-retardant solvent of trialkyl phosphoric ester by electrochemical Raman spectroscopy. In the Raman spectra, a band that peaked at around 1595 cm^{-1}, which was assigned to an E band, was observed at potentials below about 0.9 V in trimethyl phosphate (TMP)-containing electrolyte solution. After potential cycling between 3.0 and 0.01 V, several pieces of exfoliated graphite sheets were seen in the electrochemical Raman cell. On the other hand, these were not observed in triethyl phosphate (TEP)-containing electrolyte. These results indicate that TMP, unlike TEP, is co-intercalated with lithium ion into graphite, and this should lead to the observed exfoliation of graphite layers. Variation of the Raman shifts of TMP and TEP with the electrolyte composition was also investigated to discuss their different solvating abilities.

1. Introduction

The flammability of electrolyte solutions is still an important concern regarding the safety of lithium-ion batteries. Such safety issues have recently received greater attention because lithium-ion batteries are now seeing widespread use in higher-power and/or larger-size applications. Several types of flame retardants, such as organophosphorous and/or fluorinated compounds [1–9], have been shown to be effective nonflammable additives or co-solvents for use in lithium-ion batteries. Among them, trimethyl phosphate (TMP) and triethyl phosphate (TEP) suppress the flammability of electrolytes when the content is about 20% or higher in ethylene carbonate (EC) and diethyl carbonate (DEC)-based solution [10]. Unfortunately, however, TMP, unlike TEP, has poor compatibility with a graphite negative-electrode, and in particular a severe fading of capacity is seen in electrolytes containing greater than 10% TMP [11,12]. While the reaction mechanism is still unclear, several effective measures for improving the charge and discharge performances of graphite in TMP-containing electrolyte solution, such as surface coating of graphite [13,14] and the addition of film-forming additives [15,16], have been reported.

Lithium ion is intercalated into graphite negative-electrodes at the interface between an electrode and electrolyte. Laser Raman spectroscopy can detect Raman scattering near the electrode surface, and hence is a powerful tool for investigating the surface crystal structure of an electrode. Hexagonal graphite crystallizes in the D^4_{6h} space group, and has two doubly degenerate Raman-active E_{2g} modes at 42 and 1581 cm^{-1} [17]. Our group previously reported that the intensity and frequency of the E_{2g} line at around 1580 cm^{-1} varied with the intercalation and de-intercalation of lithium ion; lithium graphite intercalation compounds (Li–GICs) with a stage structure are formed [18]. It has also been revealed that the electrode potential of graphite should be determined by the surface stage of Li–GICs [18].

We previously used edge plane highly oriented pyrolytic graphite (HOPG) as a model graphite electrode, and investigated the changes in the surface crystal structure during the initial potential cycles by electrochemical Raman spectroscopy [19]. As a result, the surface crystallinity of graphite was significantly lowered by the initial intercalation and de-intercalation reactions of lithium ion in EC + DEC-based electrolyte solution, but was maintained when the film-forming additive vinylene carbonate was

* Corresponding author. Tel.: +81 774384977; fax: +81 774384996.
E-mail address: doi@saci.kyoto-u.ac.jp (T. Doi).

0378-7753/$ – see front matter © 2012 Elsevier B.V. All rights reserved.
doi:10.1016/j.jpowsour.2012.04.013

added to the electrolyte. In the present study, we observed changes in the surface structure of edge plane HOPG during the initial cycle in EC + DEC-based electrolytes containing TMP or TEP by electrochemical Raman spectroscopy, and discuss the mechanism of intercalation to understand the poor compatibility of TMP with a graphite negative-electrode.

2. Experimental

A block of HOPG (Momentive, ZYH, mosaic spread: $3.5 \pm 1.5°$) was used in this study. Cyclic voltammetry was carried out at basal plane HOPG at 25 °C using a laboratory-made three-electrode cell. The size of the HOPG block was 5 mm × 5 mm × 6 mmt. The effective electrode surface area was limited to 0.03 cm^2 by an O-ring (SS-020). The reference and counter electrodes consisted of Li foil, and hence all potentials in the text reflect *V* vs. Li/Li^+. The electrolyte solutions used were 1 M $LiClO_4$ dissolved in a mixture of EC and DEC (1:1 by volume), and did or did not include TMP (Kishida Chemical) or TEP (Kishida Chemical). The water content in the solution was less than 20 ppm. The HOPG electrode was swept at 0.5 mV s^{-1} in given potential ranges using a potentiostat/galvanostat (SP-300, Biologic).

Electrochemical Raman measurements coupled with potential sweep voltammetry were performed at edge plane HOPG. The size of the HOPG block was 8 mm × 12 mm × 2 mmt. The electrochemical cell had an airtight structure and was equipped with optically flat Pyrex® glass [20]. The HOPG was clipped between two SUS304 sheets with a hollow square with minimum pressure required for holding it, and used as a working electrode. The edge plane HOPG was irradiated with a laser beam through the Pyrex® glass to obtain Raman spectra. The distance between the HOPG surface and the Pyrex® glass was minimized to about 1 mm to suppress scattering from electrolytes. The reference and counter electrodes consisted of Li foil. The electrolyte solution described above was used. The electrochemical cell held about 50 ml of electrolyte solution. The cell was assembled in an argon-filled glove box with a dew point below −80 °C. Electrochemical lithium-ion intercalation (charge) and de-intercalation (discharge) at HOPG were carried out by controlling the potential; the HOPG electrode was swept from 3.0 to 1.0 V at 0.5 mV s^{-1}, then from 1.0 to 0.1 V at 0.2 mV s^{-1}, and finally from 0.1 to 0.01 V at 0.1 mV s^{-1}. After the electrode was held at 0.01 V for 5 h, the potential was swept in an anodic direction up to 3.0 V. Raman measurements were conducted continuously under potential control. Three accumulations of 30 s each were averaged to increase the signal-to-noise ratio, and therefore the integration time for each measurement was 90 s. This is a very short time compared to the total charging and discharging time, and hence spectral changes during each Raman measurement are considered to be negligible. Raman spectra were excited with a 632.81 nm line (50 mW) of a He–Ne laser through an objective lens: 10-powered and 100-powered long-focus objective lenses were used during potential control, and before and after potential cycling, respectively. The scattered light was collected in a backscattering (180°) geometry. The Raman spectra were recorded using a spectrometer (Horiba Jobin-Yvon, HR-800) equipped with a multichannel charge coupled device (CCD) detector. All experiments were carried out at an ambient temperature of ca. 25 °C.

Raman spectra of the solvents and solutions composed of a mixture of EC and DEC (1:1 by volume), $LiClO_4$, TMP, and/or TEP were also measured. The liquid samples were placed in a quartz cell with a pathlength of 10 mm. A 5-powered objective lens was used to focus the excitation laser on the center of the quartz cell. The exposure time was 10 s and the scattering spectrum was integrated 3 times.

3. Results and discussion

Fig. 1a shows cyclic voltammograms obtained at 0.5 mV s^{-1} in 1 M $LiClO_4$/EC + DEC containing 20 mass% TEP. A cathodic current was seen at potentials below about 1.0 V and a corresponding anodic current was observed at around 1.2 V during the anodic scan. These redox currents should be mainly attributed to the intercalation and de-intercalation of lithium ion at HOPG. The voltammogram obtained in the second cycle was very similar to that in the initial cycle except for the irreversible cathodic current at potentials ranging from 1.2 to 0.4 V, which should be due to decomposition of the electrolyte to form a surface film on the HOPG. The redox behavior was quite similar to those obtained in 1 M $LiClO_4$/EC + DEC [21]. On the other hand, in 1 M $LiClO_4$/EC + DEC containing 20 mass% TMP, a large cathodic current was observed at potentials below 0.98 V, and a corresponding anodic current appeared at around 1.05 V, as shown in Fig. 1b. These redox currents should not be assigned to the intercalation and de-intercalation of solo lithium ion at graphite because it occurs at potentials below around 0.6 V. Cyclic voltammograms similar to

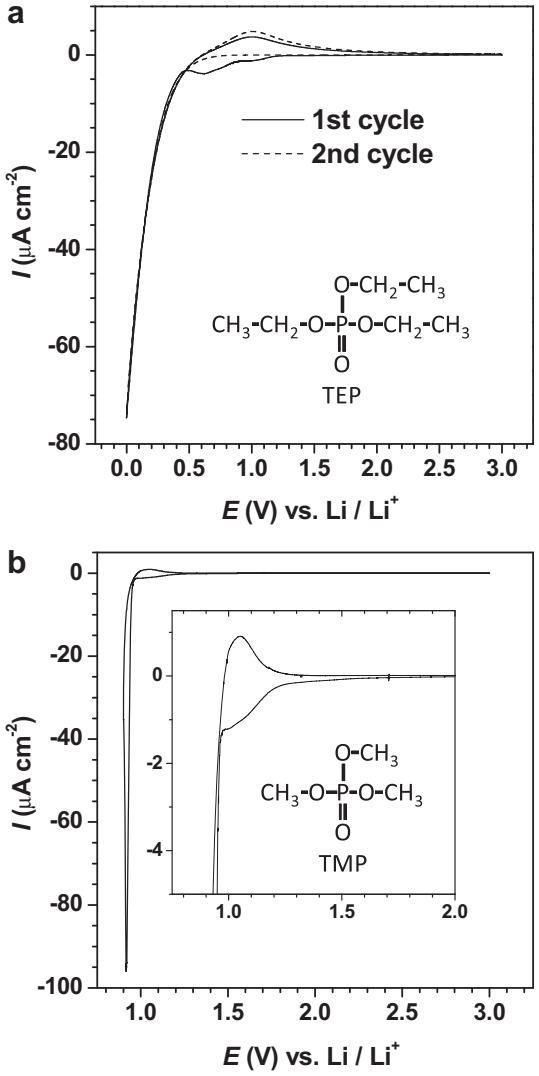

Fig. 1. Cyclic voltammograms of basal plane HOPG (a) between 0.01 and 3 V in 1 M $LiClO_4$/EC + DEC with 20 mass% TEP, and (b) between 0.9 and 3 V in 1 M $LiClO_4$/EC + DEC with 20 mass% TMP. Scan rate was 0.5 mV s^{-1}. The inset of (b) shows an expanded view of the cyclic voltammogram.

those in Fig. 1b were obtained in 1,2-dimethoxyethane (DME)- and dimethylsulfoxide (DMSO)-based electrolytes [22]; the co-intercalation of DME or DMSO with lithium ion should occur at graphite. Based on the results in the literature, the redox currents at around 1 V in Fig. 1b could be principally assigned to the intercalation and de-intercalation of lithium ion solvated by TMP. This assumption was examined by *in situ* Raman measurements (discussed later). The quantity of electricity evaluated by integrating the cathodic current at potentials below 0.98 V was more than 15 times as large as that for the anodic current. These results suggest that most of the cathodic current below 0.98 V was consumed in some irreversible reactions, which is also discussed later.

In the Raman spectrum obtained before potential cycling, a line with a peak at about 1580 cm^{-1} was observed, which is well known to be related to the crystallinity of carbonaceous materials, and is assigned to the Raman-active E_{2g} mode frequency (G band) [17]. When the electrode potential was scanned as described in the Experimental section in 20 mass% TEP-containing electrolyte solution, the G band shifted as shown in Fig. 2a; during a cathodic scan, the band at around 1580 cm^{-1} gradually shifted toward higher wavenumbers at potentials below about 1.0 V, where the cathodic current due to the intercalation of lithium ion began to flow. In this region, no lines indicative of staged phases were observed. This fact indicates that lithium ion was intercalated randomly between every layer of HOPG; i.e., a dilute stage-1 phase was formed [18,23]. The G band reached about 1590 cm^{-1} while the electrode potential was held at 0.01 V, and then two bands newly appeared on both sides of the original line. The new bands were located at about 1575 and 1600 cm^{-1} and the Raman shifts hardly changed with time. However, the intensity of these new lines increased with time, whereas that of the original line decreased. Very similar behavior was seen in EC + DEC-based electrolyte and that containing vinylene carbonate (VC) [19]. Based on the literature, the new lines were assigned to the interior and bounding layer modes of stage-4, i.e., a phase transition from dilute stage-1 to stage-4 occurred [18]. The formation of a dilute stage-1 phase and the subsequent phase transition from dilute stage-1 to stage-4 are known to occur at higher potentials above 0.2 V when a graphite electrode is charged with a constant current at a reasonably slow rate. However, in this study, these phase-changes were observed at 0.01 V because of the relatively rapid potential scan. When the electrode potential was scanned from 0.01 V in an anodic direction, the two bands disappeared immediately. Only the band at about 1590 cm^{-1} remained, and it returned to its original position of about 1580 cm^{-1} at around 0.7 V, as shown in Fig. 2a.

Fig. 2b shows the variation of the G band with the electrode potential in EC + DEC-based electrolyte solution containing 20 mass% TMP. During the initial cathodic scan, the original line remained at about 1580 cm^{-1} and a new line appeared at around 1595 cm^{-1} at about 0.9 V. However, the current flow was labile and

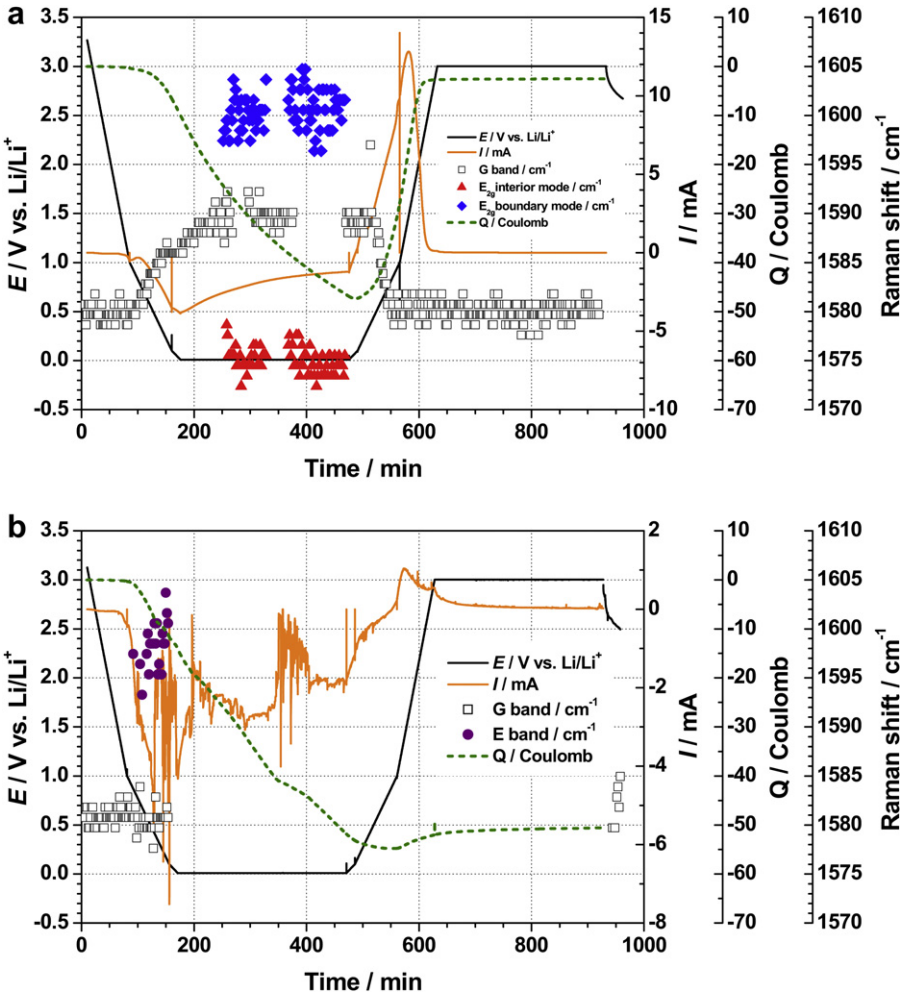

Fig. 2. Variation of the electrode potentials of edge plane HOPG, current, integrated charge amount, and Raman shift of the lines at around 1580 cm^{-1} with time in the 1st potential cycle between 3.0 and 0.01 V in 1 M $LiClO_4$/EC + DEC with 20 mass% of (a) TEP and (b) TMP.

Raman spectra could not be obtained at potentials below 0.2 V. After potential cycling, several pieces of exfoliated graphite sheets were seen in the electrochemical cell through the Pyrex® glass. These drastic changes in the electrode structure made it impossible for us to focus the exciting laser on the edge plane HOPG for *in situ* Raman measurements. Fig. 3e and f shows Raman spectra of the edge plane HOPG electrodes obtained at 3.0 V before and after potential cycling, respectively. It should be noted that a shoulder peak at about 1595 cm^{-1} was observed after potential cycling. This peak corresponds to the lines observed at around 1595 cm^{-1} in Fig. 2b. This peak was not observed in EC + DEC-based electrolyte solution or in that containing 20 mass% TEP, as shown in Fig. 3b and d, respectively [19]. This line is known to appear when solvated lithium-ion is intercalated into graphite, and is identified as an E band [24]. An E band was also observed when the edge plane HOPG was cycled in 1 M $LiClO_4$ dissolved in a mixture of EC and DME (1:1 by mass) [24], or a mixture of EC and propylene carbonate (PC) (1:1 by mass) [25]; i.e., the co-intercalation of DME or PC with lithium ion should occur at graphite. These results support the above assumption that the redox currents at around 1.0 V should be assigned to the intercalation and de-intercalation of TMP-solvating lithium-ion. The intercalation of solvated lithium-ion significantly expands the interlayer spacing of graphite [22]. The observed exfoliation of HOPG could be the result of a drastic expansion of interlayer spacing upon the intercalation of TMP-solvating lithium-ion. This irreversible change in the electrode structure may explain the large irreversible cathodic current in the cyclic voltammogram (Fig. 1b). Thus, the mechanism of lithium-ion intercalation at graphite should be different between TMP- and TEP-containing electrolytes. Another peak newly appeared at around 1310 cm^{-1} after potential cycling, as shown in Fig. 3f. This peak was seen after potential cycling in EC + DEC-based electrolyte solution and in that containing 20 mass% TEP, as shown in Fig. 3b and d, respectively, while the peak position is about 20 cm^{-1} higher than that observed in the TMP-containing electrolyte. These lines should be ascribed to the Raman inactive A_{1g} mode frequency (D band) [26]. In addition, another new peak appeared at around 1620 cm^{-1} after potential cycling in EC + DEC-based electrolyte solution and in that containing 20 mass% TEP, as shown in Fig. 3b and d, respectively, which was assigned to D′ band. The D and D′ bands appear in the case of a finite crystal size and imperfections in the carbonaceous materials [26]. The appearance of these two lines indicates that the crystallinity of the edge plane graphite should decrease during potential cycling. The other lines observed in Fig. 3 were assigned to Raman scattering from solvents and salts in the electrolytes [27,28].

Fig. 4a shows Raman spectra of solvents and solutions composed of a mixture of EC and DEC (1:1 by volume), $LiClO_4$, and/or TMP. The lines attributed to EC, DEC, TMP, and $LiClO_4$ are indicated by solid, dotted, dashed, and dashed-dotted arrows, respectively. TMP is known to have several Raman-active vibration modes [28,29]. Among them, a pair of major lines at 736 and 752 cm^{-1} and a line at 1076 cm^{-1} are sensitive to ion solvation. The former are identified as symmetric stretching vibrations of P–O–(C) in a TMP molecule, and the latter represents out-of-phase stretching vibration of (P)–O–C. These bands shifted depending on the concentration of TMP and the presence or absence of $LiClO_4$, as shown in Fig. 4a. Fig. 4b summarizes the variation of the Raman shifts

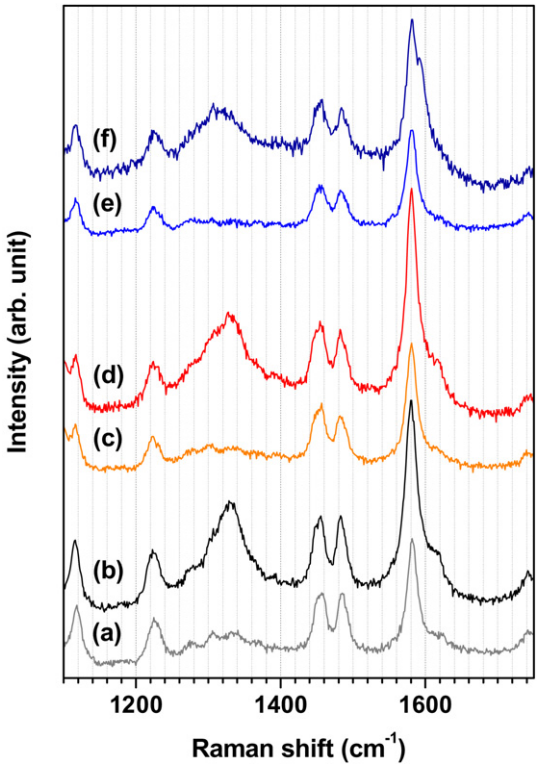

Fig. 3. Raman spectra of edge plane HOPG electrodes (a, c, e) before and (b, d, f) after potential cycling in 1 M $LiClO_4$/EC + DEC (1:1 by volume) with (a, b) no co-solvent, and 20 mass% of (c, d) TEP and (e, f) TMP.

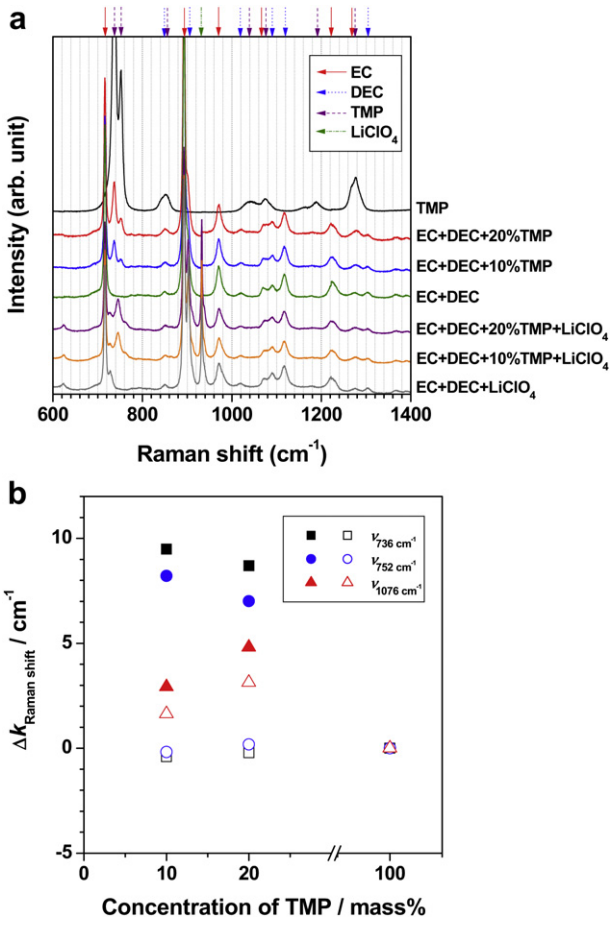

Fig. 4. (a) Raman spectra of solvents and solutions composed of a mixture of EC and DEC (1:1 by volume), $LiClO_4$, and/or TMP. (b) Variation of the Raman shift for symmetric stretching vibrations of P–O–(C) and out-of-phase stretching vibration of (P)–O–C modes with the concentration of TMP. Solid and open symbols denote solvents with and without 1 M $LiClO_4$, respectively.

($\Delta k_{\text{Raman shift}}$) with the concentration of TMP, where the value of $\Delta k_{\text{Raman shift}}$ for pure TMP solvent was set at 0 cm^{-1} for each line at 736, 752, and 1076 cm^{-1}. These bands showed few changes in $\Delta k_{\text{Raman shift}}$ even when the concentration of TMP decreased to 10–20 mass% in a solvent mixture, as shown by the open symbols in Fig. 4b, whereas the 1076 cm^{-1} band shifted by a few reciprocal centimeters (cm^{-1}). On the other hand, the three bands showed major changes in $\Delta k_{\text{Raman shift}}$ in the presence of 1 M $LiClO_4$, as shown by the solid symbols in Fig. 4b. These shifts would result from the solvation of lithium ion by TMP; the donor number generally reflects the solvent's ability to solvate cations, while it depends on the nature of the Lewis acids. The donor number of TMP is 23.0, which is much higher than 16.4 for EC and 16.0 for DEC, and therefore lithium ion should be preferentially solvated by TMP due to its higher electron-donating ability compared to those for EC and DEC [30]. An oxygen atom of a P═O bond in TMP has an unshared electron pair, and should be very involved in the solvation of lithium ion. This should alter the vibrational energies for TMP. The P–O–(C) bond lies adjacent to the P═O bond, and hence the bands at 736 and 752 cm^{-1} seem to shift upon the solvation of lithium ion. In fact, the bands at 736 and 752 cm^{-1} shifted by as much as about 7–10 cm^{-1} in the presence of 1 M $LiClO_4$. In addition, as the concentration of TMP decreased, the variation of $\Delta k_{\text{Raman shift}}$ increased, as shown in Fig. 4b; the 736 cm^{-1} band shifted by 9.9 cm^{-1} in the presence of 1 M $LiClO_4$ in 10 mass% TMP-containing solution, but by only 8.4 cm^{-1} for 20 mass% TMP. Similarly, the 752 cm^{-1} band shifted by 8.9 cm^{-1} with 1 M $LiClO_4$ in 10 mass% TMP-containing solution, but by only 6.8 cm^{-1} for 20 mass% TMP. The concentration of TMP in 1 M $LiClO_4$/EC + DEC containing 10 and 20 mass% TMP is about 0.90 and 1.8 M, respectively: i.e., the number of lithium ions is more than that of TMP in 10 mass% TMP-containing solution, but less than that for 20 mass% solution. Hence, all of the TMP molecules should be involved in solvating lithium-ion at least one-on-one in 10 mass% TMP-containing solution, while the solvation number of TMP per lithium ion is not available.

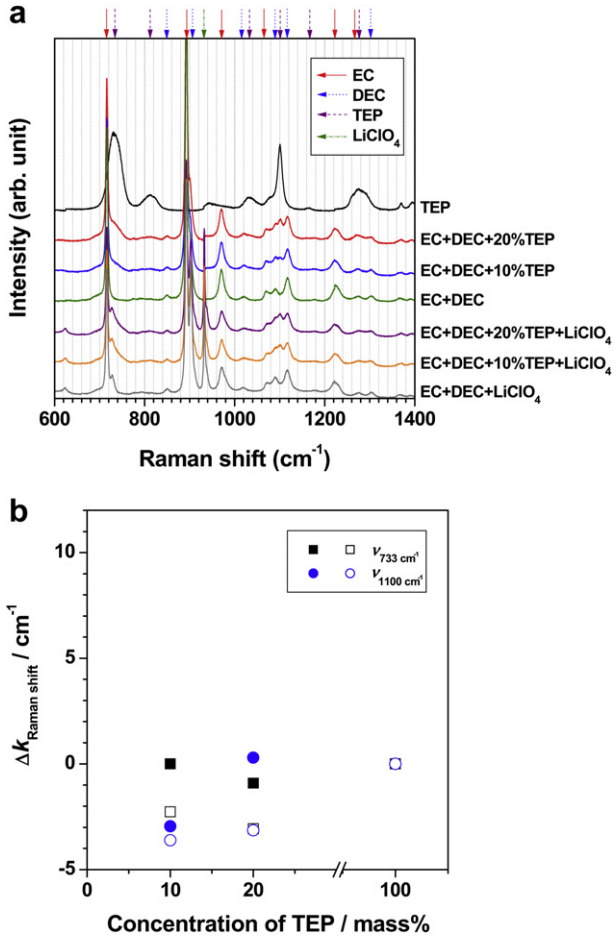

Fig. 5. (a) Raman spectra of solvents and solutions composed of a mixture of EC and DEC (1:1 by volume), $LiClO_4$, and/or TEP. (b) Variation of the Raman shift for symmetric stretching vibration of P–O–(C) and out-of-phase stretching vibration of (P)–O–C modes with the concentration of TEP. Solid and open symbols denote solvents with and without 1 M $LiClO_4$, respectively.

Fig. 5a shows Raman spectra of solvents and solutions composed of a mixture of EC and DEC (1:1 by volume), $LiClO_4$, and/or TEP. The lines attributed to EC, DEC, TEP, and $LiClO_4$ are indicated by solid, dotted, dashed, and dashed-dotted arrows, respectively. TEP also has several Raman-active vibration modes. Among them, lines at 733 and 1100 cm^{-1} are identified as the symmetric stretching vibration of P–O–(C) and out-of-phase stretching vibration of (P)–O–C, respectively. These bands, unlike in TMP-containing solutions, did not show great changes in $\Delta k_{\text{Raman shift}}$ in the presence of $LiClO_4$ in TEP-containing solutions, as shown by solid symbols in Fig. 5b; the 733 cm^{-1} band shifted by 2.3 cm^{-1} in the presence of 1 M $LiClO_4$ in 10 mass% TEP-containing solution, which is comparable to 2.2 cm^{-1} for 20 mass% TEP. Similarly, the 1100 cm^{-1} band shifted by 0.7 cm^{-1} with 1 M $LiClO_4$ in 10 mass% TEP-containing solution, whereas by 3.4 cm^{-1} for 20 mass% TEP. These results indicate that TMP should be more prone to the solvation of lithium ion than TEP, and support the co-intercalation of TMP with lithium ion into graphite.

4. Conclusion

The changes in the surface crystallinity of edge plane HOPG were observed in EC + DEC-based electrolytes containing flame-retardant solvents of TMP or TEP by electrochemical Raman spectroscopy. Raman spectra and cyclic voltammogram revealed that TMP should be co-intercalated with lithium ion into graphite at potentials below about 1.0 V. Several pieces of exfoliated graphite sheets were observed in the electrochemical cell after potential cycling. This observed exfoliation of graphite could be caused by the drastic expansion of the interlayer spacing upon the intercalation of TMP-solvating lithium-ion. On the other hand, the co-intercalation of TEP with lithium ion was not observed; lithium ion is solely intercalated and de-intercalated at graphite. Thus, the mechanism of lithium-ion intercalation at graphite differs between TMP- and TEP-containing electrolytes, and the present results clearly show that the co-intercalation of TMP into graphite precludes the use of graphite as a negative-electrode in TMP-containing electrolyte solution. Variation of the Raman shifts of TMP and TEP with the electrolyte composition was also investigated. Raman bands assigned to the P–O–(C) stretching vibrations of TMP showed major shifts in the presence of 1 M $LiClO_4$ in TMP-containing solution, while few changes were observed for TEP. These results suggest that TMP should be more prone to the solvation of lithium ion than TEP, and support the co-intercalation of TMP into graphite.

Acknowledgment

This work was supported by the New Energy and Industrial Technology Development Organization (NEDO) under contract from the Research & Development Initiative for Scientific Innovation of New Generation Batteries (RISING).

References

[1] K. Xu, S. Zhang, J.L. Allen, T.R. Jow, J. Electrochem. Soc. 149 (2002) A1079.
[2] K. Xu, M.S. Ding, S. Zhang, J.L. Allen, T.R. Jow, J. Electrochem. Soc. 150 (2003) A161.
[3] S.S. Zhang, K. Xu, T.R. Jow, J. Power Sources 113 (2003) 166.
[4] Y.E. Hyung, D.R. Vissers, K. Amine, J. Power Sources 119 (2003) 383.
[5] X.L. Yao, S. Xie, C.H. Chen, Q.S. Wang, J.H. Sun, Y.L. Li, S.X. Lu, J. Power Sources 144 (2005) 170.
[6] E.G. Shim, T.H. Nam, J.G. Kim, H.S. Kim, S.I. Moon, J. Power Sources 172 (2007) 919.
[7] T. Achiha, T. Nakajima, Y. Ohzawa, M. Koh, A. Yamauchi, M. Kagawa, H. Aoyama, J. Electrochem. Soc. 156 (2009) A483.
[8] K. Naoi, E. Iwama, N. Ogihara, Y. Nakamura, H. Segawa, Y. Ino, J. Electrochem. Soc. 156 (2009) A272.
[9] H. Nakagawa, Y. Shibata, Y. Fujino, T. Tabuchi, T. Inamasu, T. Murata, Electrochemistry 78 (2010) 406.
[10] M. Morita, Y. Niida, N. Yoshimoto, K. Adachi, J. Power Sources 146 (2005) 427.
[11] X.M. Wang, E. Yasukawa, S. Kasuya, J. Electrochem. Soc. 148 (2001) A1058.
[12] K. Xu, M.S. Ding, S. Zhang, J.L. Allen, T.R. Jow, J. Electrochem. Soc. 149 (2002) A622.
[13] X.M. Wang, E. Yasukawa, S. Kasuya, J. Electrochem. Soc. 148 (2001) A1066.
[14] X.M. Wang, C. Yamada, H. Naito, G. Segami, K. Kibe, J. Electrochem. Soc. 153 (2006) A135.
[15] H. Ota, A. Kominato, W.-J. Chun, E. Yasukawa, S. Kasuya, J. Power Sources 119–121 (2003) 393.
[16] N. Yoshimoto, Y. Niida, M. Egashira, M. Morita, J. Power Sources 163 (2006) 238.
[17] R.J. Nemanich, G. Lucovsky, S.A. Solin, Solid State Commun. 23 (1977) 117.
[18] M. Inaba, H. Yoshida, Z. Ogumi, T. Abe, Y. Mizutani, M. Asano, J. Electrochem. Soc. 142 (1995) 20.
[19] H. Nakagawa, Y. Domi, T. Doi, M. Ochida, S. Tsubouchi, T. Yamanaka, T. Abe, Z. Ogumi, J. Power Sources 206 (2012) 320.
[20] M. Inaba, H. Yoshida, Z. Ogumi, J. Electrochem. Soc. 143 (1996) 2572.
[21] Y. Domi, M. Ochida, S. Tsubouchi, H. Nakagawa, T. Yamanaka, T. Doi, T. Abe, Z. Ogumi, J. Phys. Chem. C 115 (2011) 25484.
[22] T. Abe, H. Fukuda, Y. Iriyama, Z. Ogumi, J. Electrochem. Soc. 151 (2004) A1120.
[23] G.L. Doll, P.C. Eklund, J.E. Fischer, Phys. Rev. B 36 (1987) 4940.
[24] W. Huang, R. Frech, J. Electrochem. Soc. 145 (1998) 765.
[25] L.J. Hardwick, H. Buqaa, M. Holzapfel, W. Scheifele, F. Krumeich, P. Novák, Electrochim. Acta 52 (2007) 4884.
[26] F. Tuinstra, J.L. Koenig, J. Chem. Phys. 53 (1970) 1126.
[27] B. Klassen, R. Aroca, J. Phys. Chem. B 102 (1998) 4795.
[28] F.S. Mortimer, Spectrochim. Acta 9 (1957) 270.
[29] A. Simon, G. Schulze, Naturwissenschaften 25 (1937) 669.
[30] H. Tsunekawa, A. Narumi, M. Sano, A. Hiwara, M. Fujita, H. Yokoyama, J. Phys. Chem. B 107 (2003) 10962.